EUROPEAN ORGANIZATION FOR NUCLEAR RESEARCH

CERN-EP/83-90
5 July 1983

A COMPARISON OF TWO-PARTICLE RAPIDITY CORRELATIONS IN ANTIPROTON-PROTON AND PROTON-PROTON INTERACTIONS AT 31 GeV CENTRE-OF-MASS ENERGY

V. Cavasinni[1], T. Del Prete, M. Morganti, F. Schiavo and
M. Valdata-Nappi[2]
INFN and Istituto di Fisica dell'Università, Pisa, Italy

G. Carboni[3] and D. Lloyd Owen
CERN, Geneva, Switzerland

M. Ambrosio, G. Barbarino, G. Paternoster and S. Patricelli
Istituto di Fisica dell'Università and INFN, Naples, Italy

G. Anzivino[4]
State University of New York, Stony Brook, NY, USA

(Submitted to Zeitschrift für Physik C)

---

[1] Also at Scuola Normale Superiore, Pisa, Italy.
[2] Present address: ANL, Argonne, IL, USA.
[3] On leave of absence from INFN, Pisa, Italy.
[4] Also at Istituto di Fisica dell'Università and INFN, Naples, Italy.

$\bar{p}p$ and pp rapidity correlations

Abstract: We investigated correlations between pairs of charged secondaries produced in antiproton-proton and proton-proton interactions at a centre-of-mass energy of 31 GeV using the pseudorapidity variable $\eta = -\ln(\tan\theta/2)$. Positive, short-range correlations were observed in both reactions. In the antiproton-proton case, however, there is a stronger correlation at very short range when both particles are produced in the central region and when the charged multiplicity of the event is about 30% higher than the mean. A simple Monte Carlo calculation indicates that quark-antiquark annihilation into two hadronic jets could account for the observed effect.

1. INTRODUCTION

It is commonly held that the differences between antiproton-proton and proton-proton interactions will vanish at asymptotic energies. At the highest energies where both reactions can be studied (i.e. at the CERN Intersecting Storage Rings), differences in terms of total and elastic cross-sections -- whilst diminishing -- are still appreciable [1-5]. In this letter, we shall show that differences in multiparticle production also persist to ISR energies.

At low energy, the differences between $\bar{p}p$ and pp reactions can be ascribed to the annihilation channel [6]. In contrast to the soft, "peripheral" processes common to both $\bar{p}p$ and pp interactions, annihilation is a very inelastic process, and one expects that this should be manifested in the final-state topologies of $\bar{p}p$ collisions. A comparative study of multiparticle production is, therefore, a potentially fruitful way of expanding our understanding of the persisting $\bar{p}p$/pp differences.

Results on multiplicity and single-particle distributions [7,8] and on two-body correlations [9,10] in $\bar{p}p$ and pp collisions at the ISR have already been reported. Within the accuracy of these measurements, no

clear difference in the two reactions was apparent. When the correlations are considered in terms of second-order (Bose-Einstein) interference, however, there is some evidence of differences between the two reactions [10].

In this communication, we present the results of an analysis of secondary production in $\bar{p}p$ and pp collisions at the centre-of-mass energy $\sqrt{s}$ = 31 GeV in terms of the two-particle correlation function. Earlier measurements of this quantity in pp collisions at the ISR [11-15] showed that secondaries are not emitted independently, but are found to cluster in rapidity over a range of about two units (short-range correlations). This correlation is commonly understood as being due to the independent production of low-mass objects which subsequently decay into few particles [16,17].

2. THE EXPERIMENT

The apparatus -- the same as that used for the measurement of the total cross-section -- has been described in detail elsewhere [1,2]. Briefly, it consisted of a set of scintillation-counter trigger hodoscopes which covered almost 100% of the full solid angle. The fully inclusive trigger, which required at least one detected charged particle in each hemisphere, was sensitive to about 99% of all inelastic events. Single-beam background, originating in the collisions of beam protons with the vacuum chamber or with the residual gas, was quite severe in $\bar{p}p$ runs because of the very asymmetric currents and the low luminosity. It was minimized by using a small-angle trigger, more restrictive than the fully inclusive trigger but still sensitive to about 75% of all inelastic events. Timing information provided by the hodoscopes could be used off-line to reduce background contamination of the data to < 3%.

Two different systems were used for the detection of charged secondaries:

- hodoscopes of scintillation counters, which covered the entire azimuth in the pseudorapidity range $|\eta| < 5$ but which had poor η and ϕ resolution, and
- a drift-chamber vertex detector, which had a much better η resolution

but covered a more limited polar range ($|\eta| < 2$).

The scintillator hodoscopes were divided into annular rings with a width in η ranging from 0.5 units in the central region to 0.1 units at small angles. The rings were subdivided into quadrants or octants in azimuthal angle.

The vertex detector (described in detail in Ref. 18) was operated in the absence of a magnetic field, and so no measurements of momentum or charge sign were performed. The system had a resolution in η of 0.05 units in the central region. In the analysis performed with the chambers, the interaction vertex was reconstructed with a spatial resolution of $< \pm 10$ mm; thus all background events were positively identified. About 70% of all inelastic events survived the fiducial cuts imposed on the vertex distribution.

The $\bar{p}p$ data were collected with currents of 2-4 mA for $\bar{p}$'s and 10 A for p's, yielding an instantaneous luminosity of 10^{26}-10^{27} cm^{-2} s^{-1} and an integrated luminosity of $4\text{-}7\times10^{32}$ cm^{-2}. In order to minimize systematic biases, the pp data were taken immediately before the $\bar{p}p$ run at the corresponding energy.

The correlation function obtained after integrating over azimuthal angle is defined by the following expression:

$$R_2(\eta_1,\eta_2) = [\rho_2(\eta_1,\eta_2)]/[\rho_1(\eta_1) \cdot \rho_1(\eta_2)] - 1 ,$$

where $\rho_2(\eta_1,\eta_2)$ is the two-particle density at (η_1,η_2), and $\rho_1(\eta)$ is the single-particle density at η. In terms of directly measured quantities, R_2 can be written:

$$R_2(\eta_1,\eta_2) = [N_{inel} \cdot N_2(\eta_1,\eta_2)]/[N_1(\eta_1) \cdot N_1(\eta_2)] - 1 ,$$

where N_{inel} is the measured counting rate of inelastic collisions, $N_1(\eta)$ is the rate of a single charged particle at η, and $N_2(\eta_1,\eta_2)$ is the rate of two charged particles, one at η_1 and one at η_2, in the same event. If particles are emitted independently, $R_2(\eta_1,\eta_2)$ is zero.

Note that $R_2(\eta_1,\eta_2)$ is insensitive to many experimental biases, to first order, because it is a ratio of experimental rates. Secondary interactions in the ambient material surrounding the interaction region could, however, have affected the value of R_2. In addition to being small, such effects are expected to be the same for both $\bar{p}p$ and pp reactions on the basis of the similarity of their measured secondary distributions, and, consequently, no corrections were made.

3. THE RESULTS

First, let us consider the scintillation-counter data. In Fig. 1 we present $R_2(\eta_1,\eta_2)$ as a function of η_2, with η_1 held fixed at $\eta_1 = 0.25$ for both $\bar{p}p$ and pp collisions. Within the accuracy of the measurement, no difference between $\bar{p}p$ and pp is apparent. The figures exhibit the familiar positive short-range correlation peaking at $\eta_1 = \eta_2$, in good agreement with a previous measurement performed at the ISR [11].

Let us now turn to the chamber data. We shall see that, although the statistics of these data is poorer (we analysed about 30 000 chamber events compared with 100 000 counter events for each reaction), the better η resolution of the chambers was essential.

Figure 2 again shows $R_2(\eta_1,\eta_2)$ as a function of η_2 for $\bar{p}p$ and pp collisions, this time for six regions of fixed η_1. Let us first examine Fig. 2c, in which the region of fixed η_1 corresponds to that in Fig. 1.

The data presented in Figs. 1 and 2c are broadly similar, except that the height of the maxima at $\eta_1 = \eta_2$ are slightly lower for the chamber data. This is an artefact of the different event-selection criteria for the two sets of data. The most striking aspect of Fig. 2c is the excess of correlation, at the maximum of the $\bar{p}p$ distribution, that emerges with the

improved resolution of the chamber data. This excess of correlation is limited to a range in η_2 of about ± 0.3 units (hence its apparent absence in the counter data). Reducing by a factor of 2 the η_1 interval over which R_2 was integrated, we found no appreciable change in the width of the $\bar{p}p$ excess in η_2 -- it is much narrower than the short-range correlations common to both reactions, and, consequently, indicative of a separate dynamical mechanism.

In order to be certain that the effect was not due to secondary interactions, we reanalysed the data, imposing more stringent cuts on the reconstructed vertex, thus improving the identification and rejection of secondary vertices. The extra $\bar{p}p$ correlation was not affected.

To investigate the correlation as a function of the rapidities of both charged particles, we calculated $R_2(\eta_1,\eta_2)$ for the other values of fixed η_1 shown in Fig. 2. Both $\bar{p}p$ and pp correlation functions have maxima at $\eta_1 = \eta_2$, as expected from earlier pp correlation studies. The $\bar{p}p$ excess, however, diminishes as η_1 moves away from zero. In order to quantify the η_1 dependence of the extra $\bar{p}p$ correlation, we integrated the difference $\Delta R_2 = R_2(\bar{p}p) - R_2(pp)$ over η_2 at each η_1 setting and plotted this difference as a function of η_1. The results are shown in Fig. 3: one sees clearly that the enhancement of the $\bar{p}p$ correlation function occurs only for

$-1 < \eta_1 \approx \eta_2 < 1$.

We then investigated the correlation semi-inclusively, i.e. in different multiplicity ranges. The pp multiplicity distribution has already been measured at the ISR [19]. We found that the $\bar{p}p$ distribution is broadly similar with a mean 2% higher than in the pp case [20,21]. The distribution in the difference of the topological cross-sections -- which we shall refer to as the annihilation distribution -- peaks at a multiplicity 30% higher than in the $\bar{p}p$ and pp distributions from which it is derived, although it has a similar Gaussian shape. We separated our data into three multiplicity ranges with reference to the mean annihilation multiplicity N_{ann}: $n_{ch} < 2/3\ N_{ann}$; $2/3\ N_{ann} < n_{ch} < 4/3\ N_{ann}$; and $4/3\ N_{ann} < n_{ch}$.

The semi-inclusive correlation functions for both reactions are shown in Fig. 4 for these multiplicity ranges. The $\bar{p}p$ enhancement is visible only in the middle range, indicating that not all $\bar{p}p$ inelastic events give this extra correlation, but only the subsample where the number of produced particles is larger than the average pp or $\bar{p}p$ multiplicity, i.e. around the mean value of the annihilation multiplicity.

Finally, we examined the data to see if there was an azimuthal correlation associated with the $\bar{p}p$ excess in the pseudorapidity correlation. We

calculated $R_2(\phi_1,\phi_2)$ (defined analogously to $R_2[\eta_1,\eta_2]$) at fixed ϕ_1 for pairs of tracks. The results are shown in Fig. 5: a) for all events, and b) for medium-multiplicity events considering only tracks in the range $|\eta| < 1$. In both cases there is no apparent difference between $\bar{p}p$ and pp: both reactions show the observed [16] positive correlation for $\Delta\phi = 0$ and $\Delta\phi = \pi$.

The features of $\bar{p}p$ and pp correlations discussed above show that, in addition to the observed persisting difference in total cross-sections, there are also differences in the final-state topologies at ISR energies. In this letter, we have reported the effect as seen at $\sqrt{s} = 31$ GeV, where the total cross-section difference is the largest measured at the ISR. We have also investigated our 53 GeV and 63 GeV data for differences in two-body correlations between $\bar{p}p$ and pp: at all energies, the excess of $\bar{p}p$ correlation is present with properties similar to those we have reported at 31 GeV. (The s dependence of the effect is currently under investigation.)

The effect can be summarized as follows:

- in $\bar{p}p$ inelastic interactions, the particles produced are more correlated than in pp interactions;
- the extra component of correlation is superimposed on the maximum at $\eta_1 \approx \eta_2$, and has a width $\eta_1 - \eta_2 \approx \pm 0.3$ units;

- this excess is confined to the central region $-1 < \eta_1 \approx \eta_2 < 1$;
- it is present predominantly in that subset of events with charged multiplicity corresponding to the mean of the annihilation multiplicity distribution; and
- no extra azimuthal correlation is associated with the rapidity effect.

The cause of this effect is not obvious. In the language of Regge-pole theory, rapidity correlation lengths are related to the difference between the Pomeron intercept and the intercept of the next leading pole: correlation length, $\xi = [\alpha_P - \alpha_R]^{-1}$. The ρ and ω odd charge-conjugation poles, which are associated with the $\bar{p}p$ - pp total cross-section difference, have intercepts of $\alpha_\rho \approx \alpha_\omega \approx 0.5$, giving a correlation length $\xi \approx 2$ -- too large compared with the observed value of 0.3. Even the lowest-lying baryon trajectory (with $\alpha_N = -0.3$) gives $\xi \approx 0.7$, which is still too large.

In the framework of quantum chromodynamics (QCD), one might expect that quark-antiquark annihilation into quark or gluon pairs would play a more important role in $\bar{p}p$ collisions than it does in pp, and, in that case, yield extra events in which two jets of particles are emitted. Owing to the balanced quark and antiquark structure functions in the proton and in the antiproton, this production would be central in rapidity.

Motivated by these ideas, we performed a naive Monte Carlo calculation to see if quark-antiquark annihilation could be the source of the extra correlation. The Monte Carlo simply took pp events from our data, superimposed two jets on a variable fraction of the events, and then calculated the associated correlation function. The jets were generated centrally in rapidity and back-to-back in azimuth, and their properties (mean multiplicity, $\langle n_{jet} \rangle = 2$; mean opening angle of jet $\langle \Delta\omega_{jet} \rangle = 20^0$) were taken from results on e^+e^- annihilation into hadrons [22]. It is interesting to note that 20^0, the mean opening angle of jets in e^+e^- collisions, is equivalent to a rapidity of $\Delta\eta \approx \pm 0.3$ in the central region, i.e. the width of the excess in the $\bar{p}p$ correlation.

The results are shown in Fig. 6: the open circles represent the input pp data; the full circles represent the Monte Carlo calculation when the two jets are superimposed on 1 in every 70 events. Comparison of this figure with Fig. 2c shows that this simplified model can indeed reproduce the excess of $\bar{p}p$ correlation that is observed.

The Monte Carlo also calculates the azimuthal correlation function; the result is presented in Fig. 7 as is the correlation function derived from the input data. This is to be compared with Fig. 5a: the superimposition of jets on a small fraction of pp events has no effect on the azimuthal

correlation, and the model calculation is again in agreement with our $\bar{p}p$ data. In the central region, the particles of two back-to-back jets are all close in rapidity, whereas in azimuth it is only within each jet that particles cluster. This explains the presence of a polar correlation in the absence of an azimuthal one.

The cross-section associated with this frequency of jet production is not, however, sufficient to account for the entire $\bar{p}p$ - pp total cross-section difference, but only a fraction of it (15-20%). This suggests that, whilst single $\bar{q}q$ annihilation into hadron jets is a significant mechanism in the difference between $\bar{p}p$ and pp interactions, it is not the only mechanism.

ACKNOWLEDGEMENTS

The advice and assistance of P.D. Grannis at all stages of the experiment are warmly appreciated. The tireless efforts of T. Regan in assembling, installing, testing, and maintaining the chamber electronics were essential to this measurement. The technical assistance of G.C. Barnini, A. Bechini, and L. Giacomelli is gratefully acknowledged. We also wish to thank Mme R. Dubos-Latrauguère for the administrative help she has provided during the course of the experiment.

REFERENCES

[1] G. Carboni et al., Phys. Lett. 108B (1982) 145.
[2] G. Carboni et al., Phys. Lett. 113B (1982) 87.
[3] M. Ambrosio et al., Phys. Lett. 115B (1982) 495.
[4] D. Favart et al., Phys. Rev. Lett. 47 (1981) 1191.
[5] N. Amos et al., Phys. Lett. 120B (1983) 460.
[6] J.G. Rushbrooke et al., Phys. Lett. 59B (1975) 303.
[7] T. Åkesson et al., Phys. Lett. 108B (1982) 58.
[8] K. Alpgard et al., Phys. Lett. 112B (1982) 183.
[9] A. Breakstone et al., Phys. Lett. 114B (1982) 383.
[10] G. Giacomelli, University of Bologna preprint IFUB 82/23 (1982).
[11] S.R. Amendolia et al., Phys. Lett. 48B (1974) 359.
[12] L. Foà, Phys. Rep. 22C (1975) 1.
[13] T. Del Prete, Rivista del Nuovo Cimento 5 (1975) 532.
[14] G. Giacomelli and M. Jacob, Phys. Rep. 55 (1979) 1.
[15] D. Drijard et al., Nucl. Phys. B155 (1979) 269.
[16] K. Eggert et al., Nucl. Phys. B86 (1975) 201.
[17] S.R. Amendolia et al., Nuovo Cimento 31A (1976) 17.
[18] A. Bechini et al., Nucl. Instrum. Methods 156 (1978) 181.
[19] W. Thomé et al., Nucl. Phys. B129 (1977) 365.
[20] G. Carboni, Proc. Third Topical Workshop on Proton-Antiproton Collider Physics, Rome, 1983, eds. C. Bacci and G. Salvini (CERN 83-04, Geneva, 1983), p.251.
[21] V. Cavasinni, talk given at the Moriond Workshop on Antiproton Physics, La Plagne, France, 19-25 March 1983 (proceedings, ed. J. Tran Thanh Van, to be published).
[22] G. Hanson et al., Phys. Rev. Lett. 35 (1975) 1609.

FIGURE CAPTIONS

Fig. 1: $R_2(\eta_1,\eta_2)$ versus η_2 for fixed η_1 in $\bar{p}p$ and pp interactions at $\sqrt{s}$ = 31 GeV (scintillation-counter data).

Fig. 2: $R_2(\eta_1,\eta_2)$ versus η_2 for six regions of fixed η_1 in $\bar{p}p$ and pp interactions at $\sqrt{s}$ = 31 GeV (drift-chamber data): a) $-1.44 < \eta_1 < -0.84$; b) $-0.84 < \eta_1 < -0.36$; c) $-0.36 < \eta_1 < 0.12$; d) $0.12 < \eta_1 < 0.60$; e) $0.60 < \eta_1 < 1.08$; and f) $1.08 < \eta_1 < 1.56$.

Fig. 3: The ($\bar{p}p$ - pp) difference in $R_2(\eta_1,\eta_2)$ integrated over η_2 and plotted as a function of η_1 at $\sqrt{s}$ = 31 GeV.

Fig. 4: The semi-inclusive correlation function in $\bar{p}p$ and pp interactions at 31 GeV for a) $n_{ch} < 2/3\ N_{ann}$; b) $2/3\ N_{ann} < n_{ch} < 4/3\ N_{ann}$; and c) $4/3\ N_{ann} < n_{ch}$.

Fig. 5: The azimuthal correlation function $R_2(\phi_1,\phi_2)$ versus ϕ_2 for fixed ϕ_1 at $\sqrt{s}$ = 31 GeV: a) for all events, and b) for medium multiplicity events and $|\eta| < 1$.

Fig. 6: Model calculation of the $\bar{p}p$ pseudorapidity correlation. The open circles are pp data taken as input, the full circles are the results of the jet Monte Carlo (see text).

Fig. 7: Model calculation of the $\bar{p}p$ azimuthal correlation. The open circles are pp data taken as input, the full circles are the results of the jet Monte Carlo (see text).

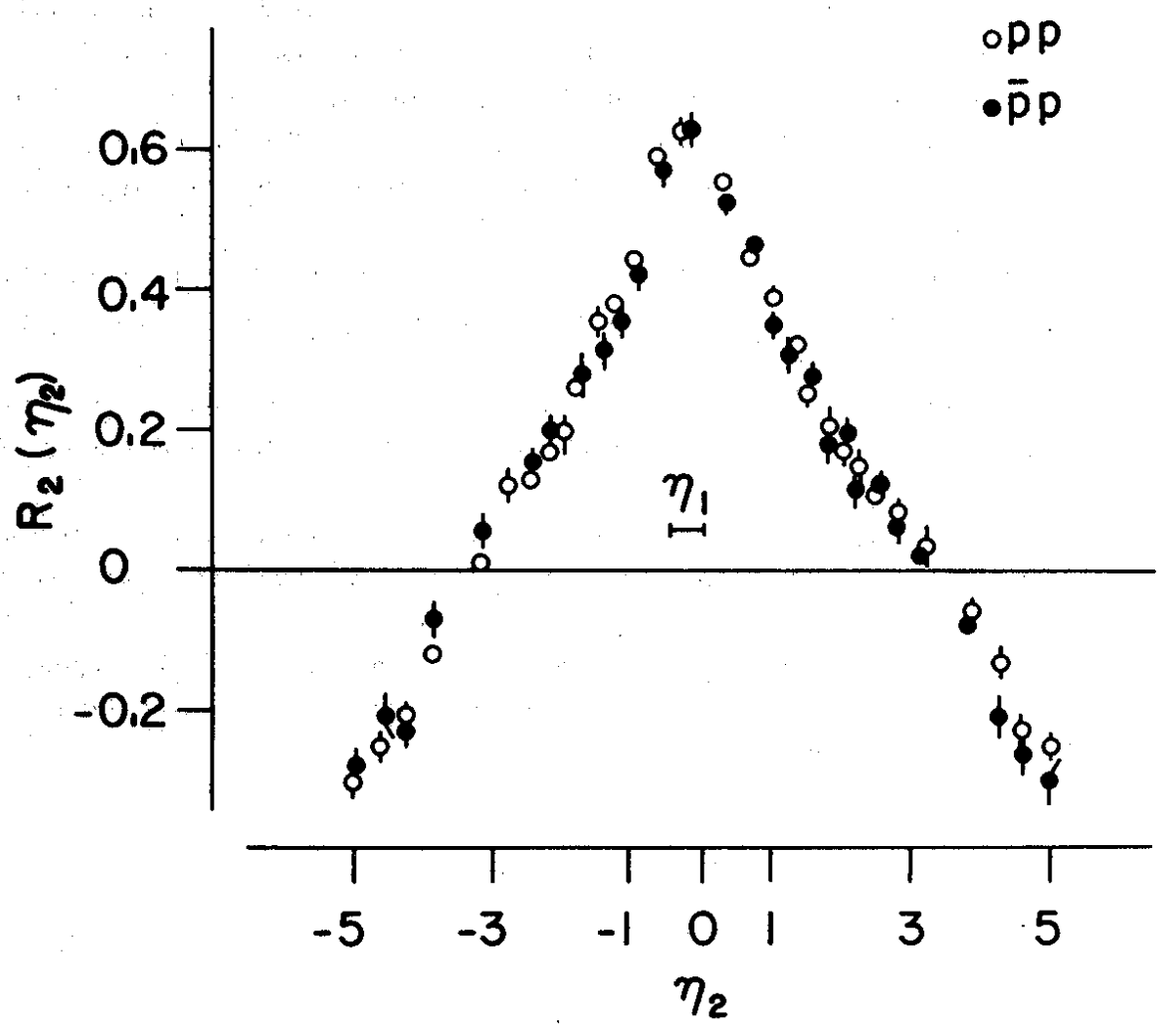

Fig. 1

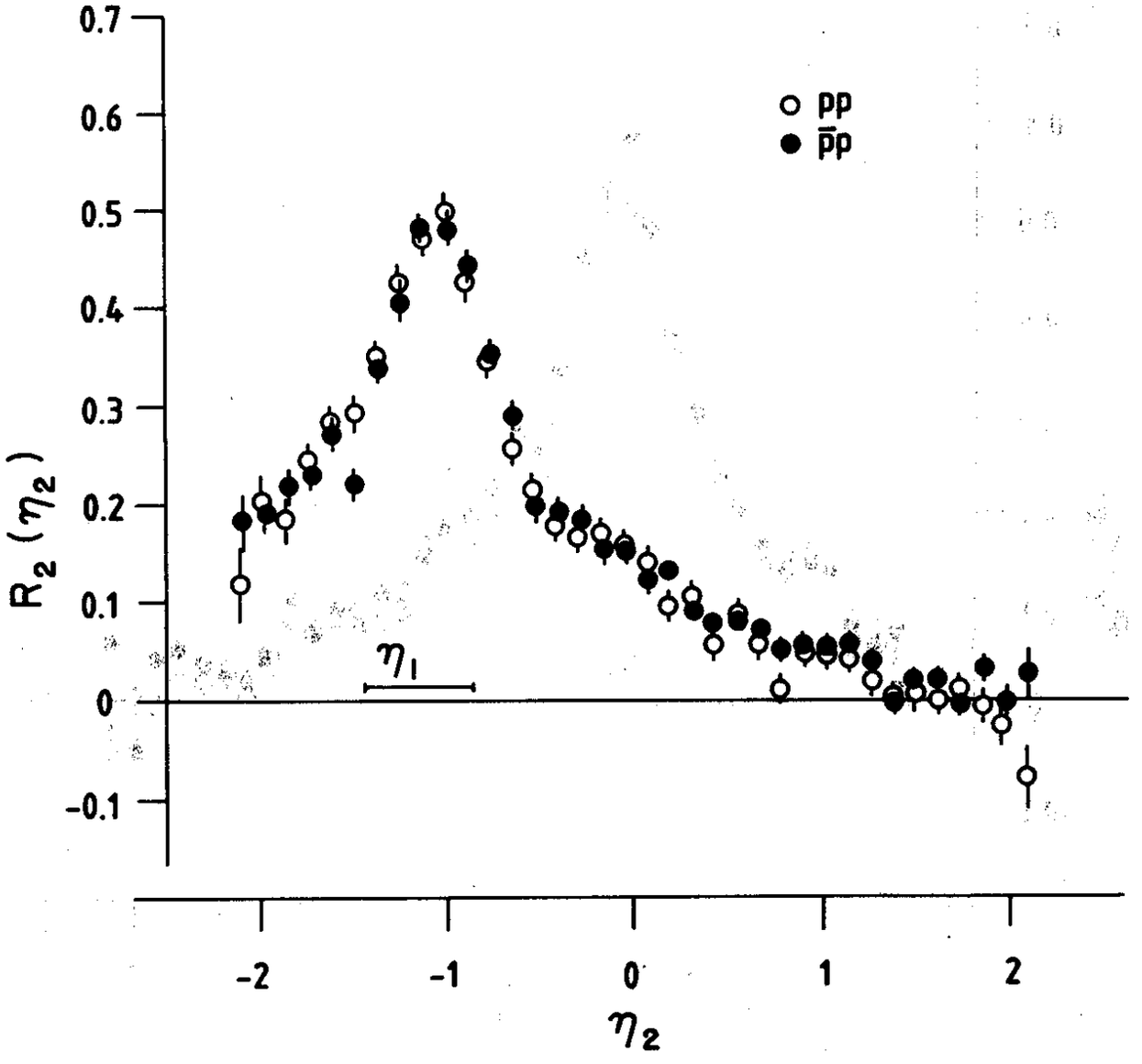

Fig. 2a

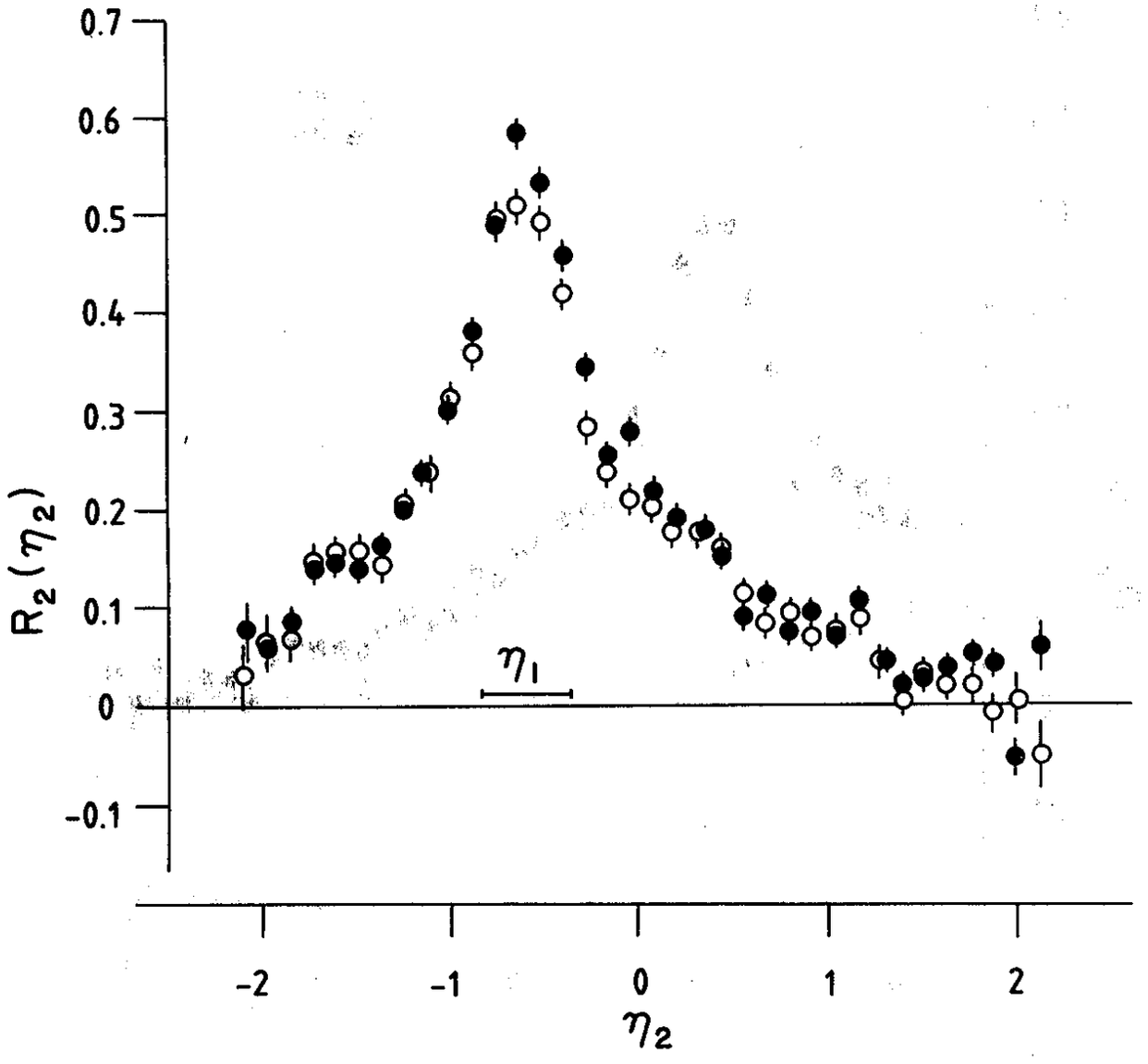

Fig. 2b

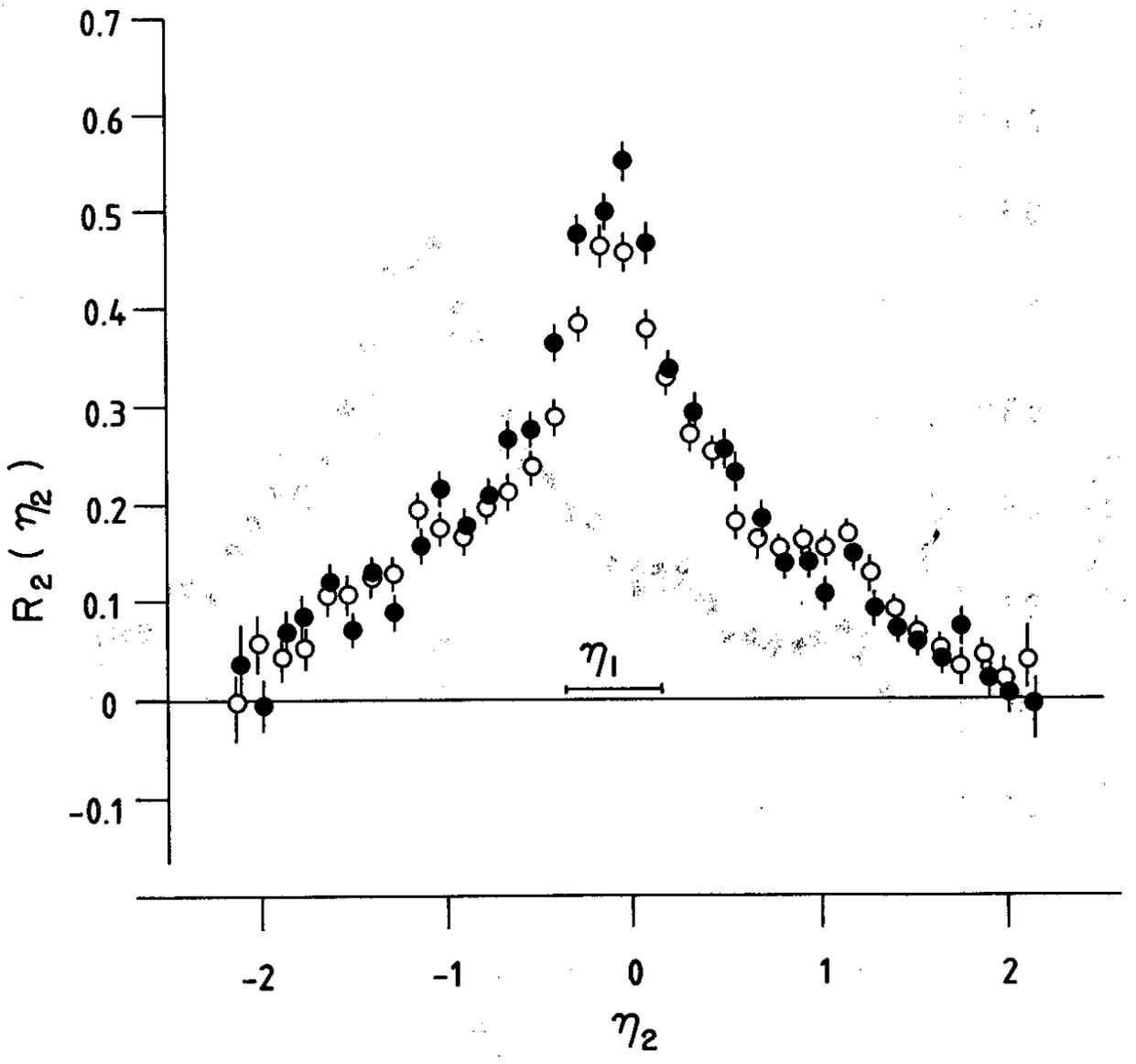

Fig. 2c

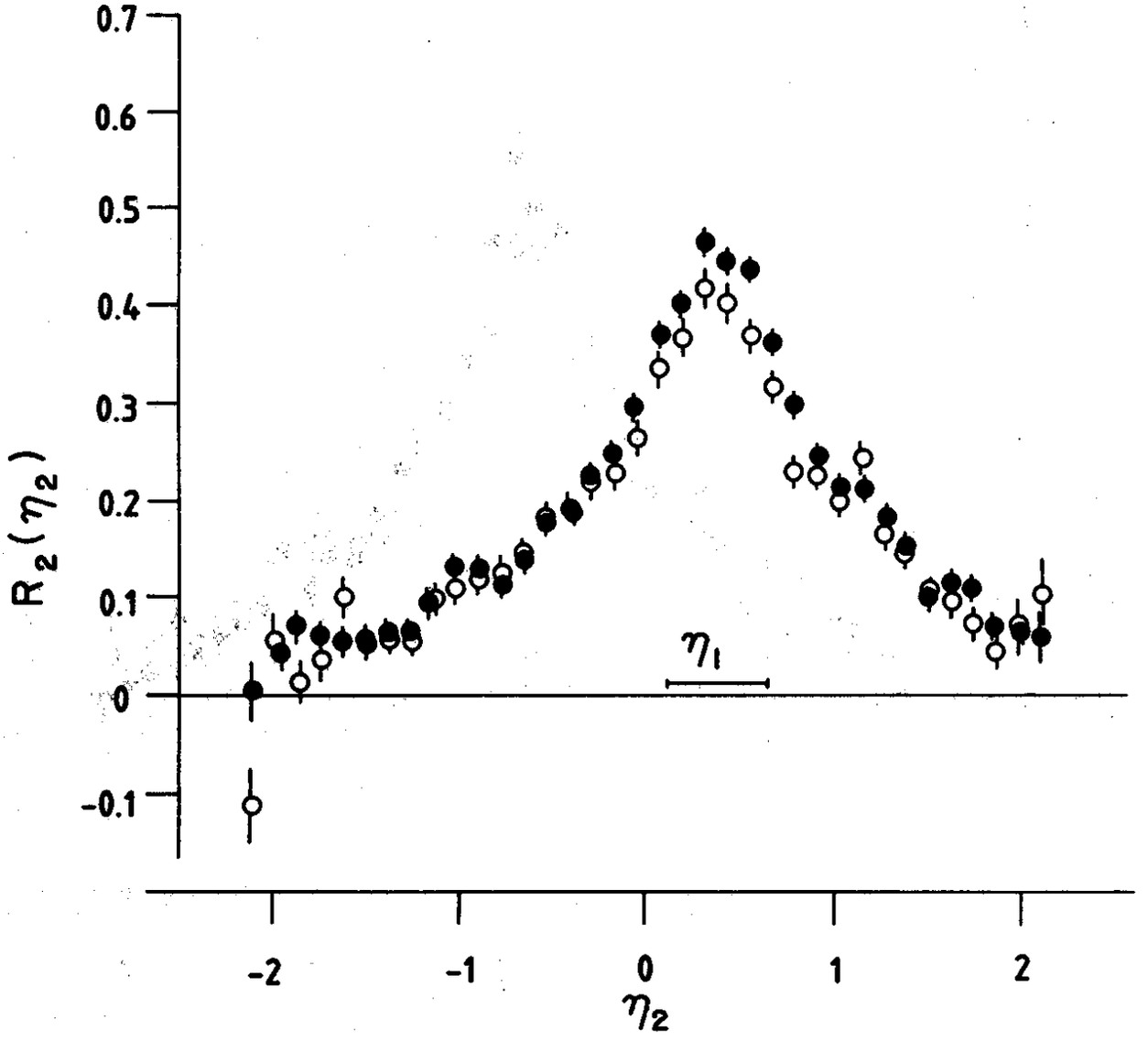

Fig. 2d

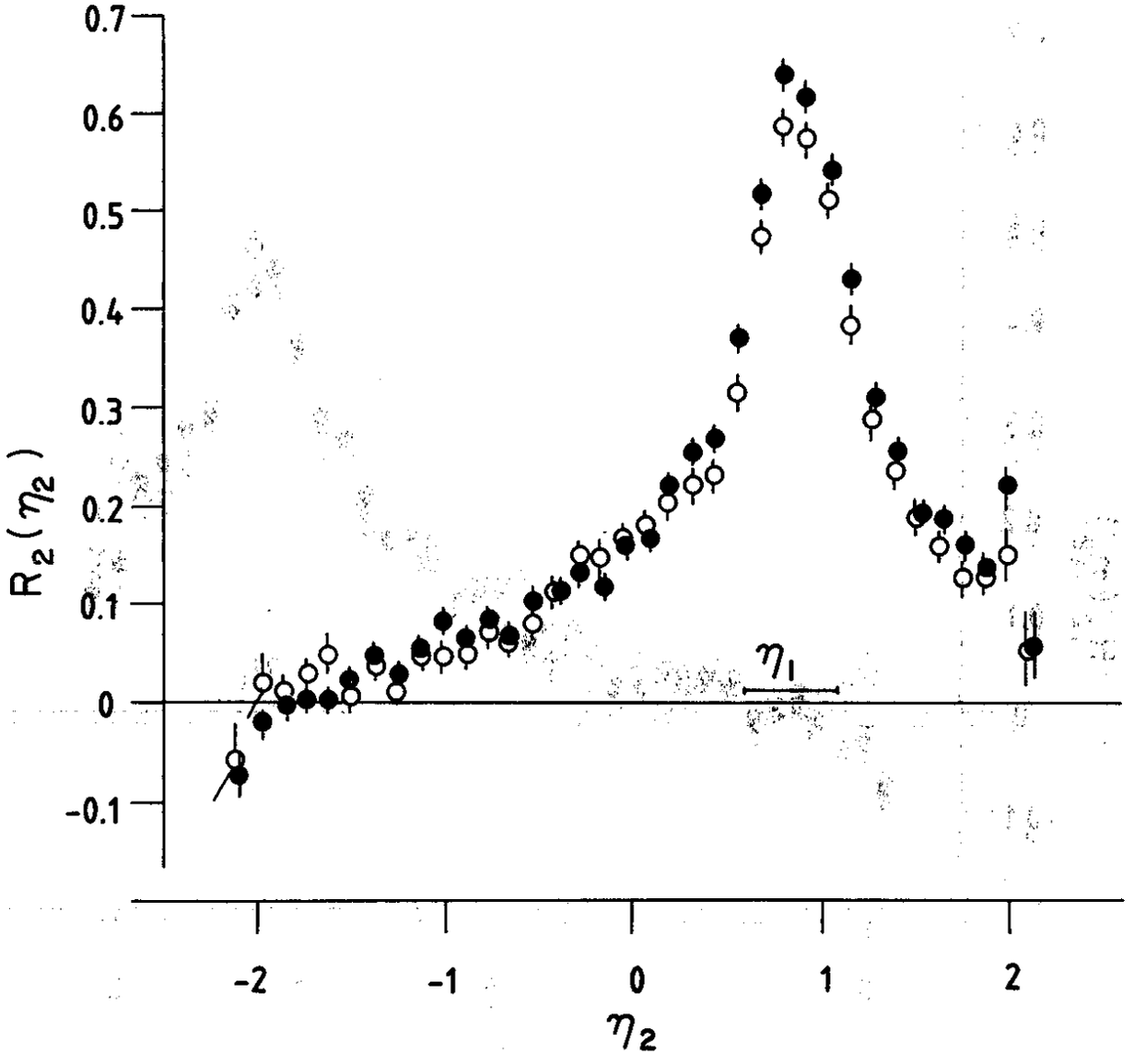

Fig. 2e

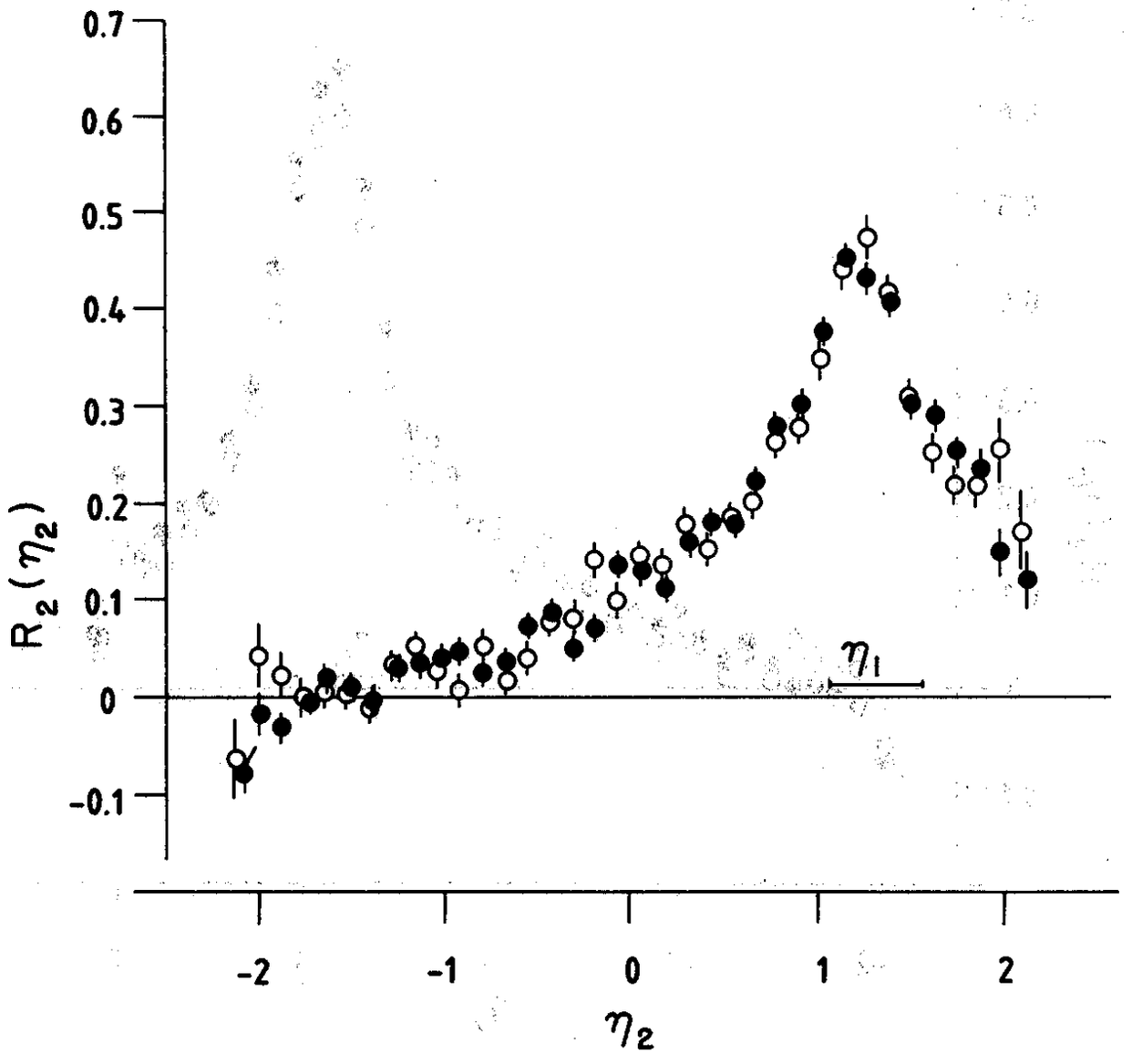

Fig. 2f

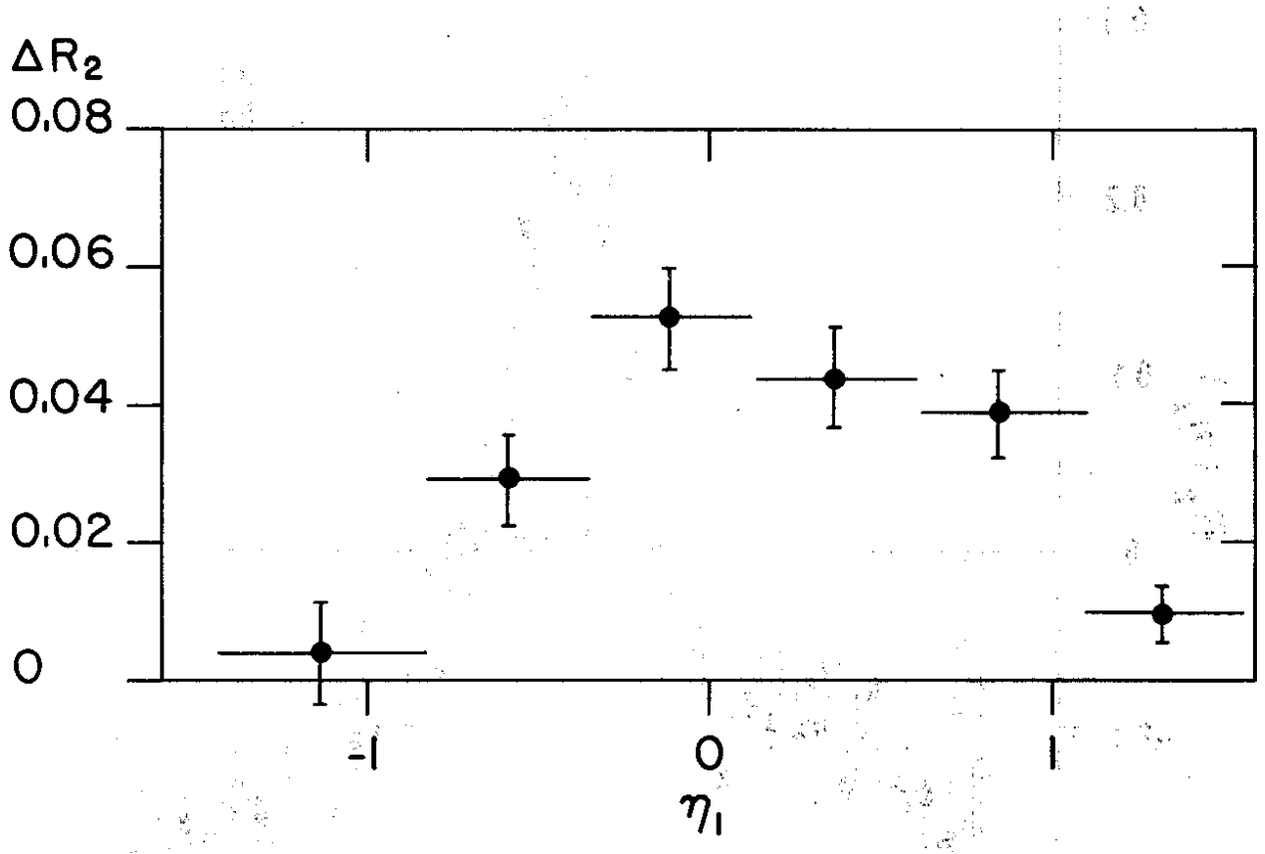

Fig. 3

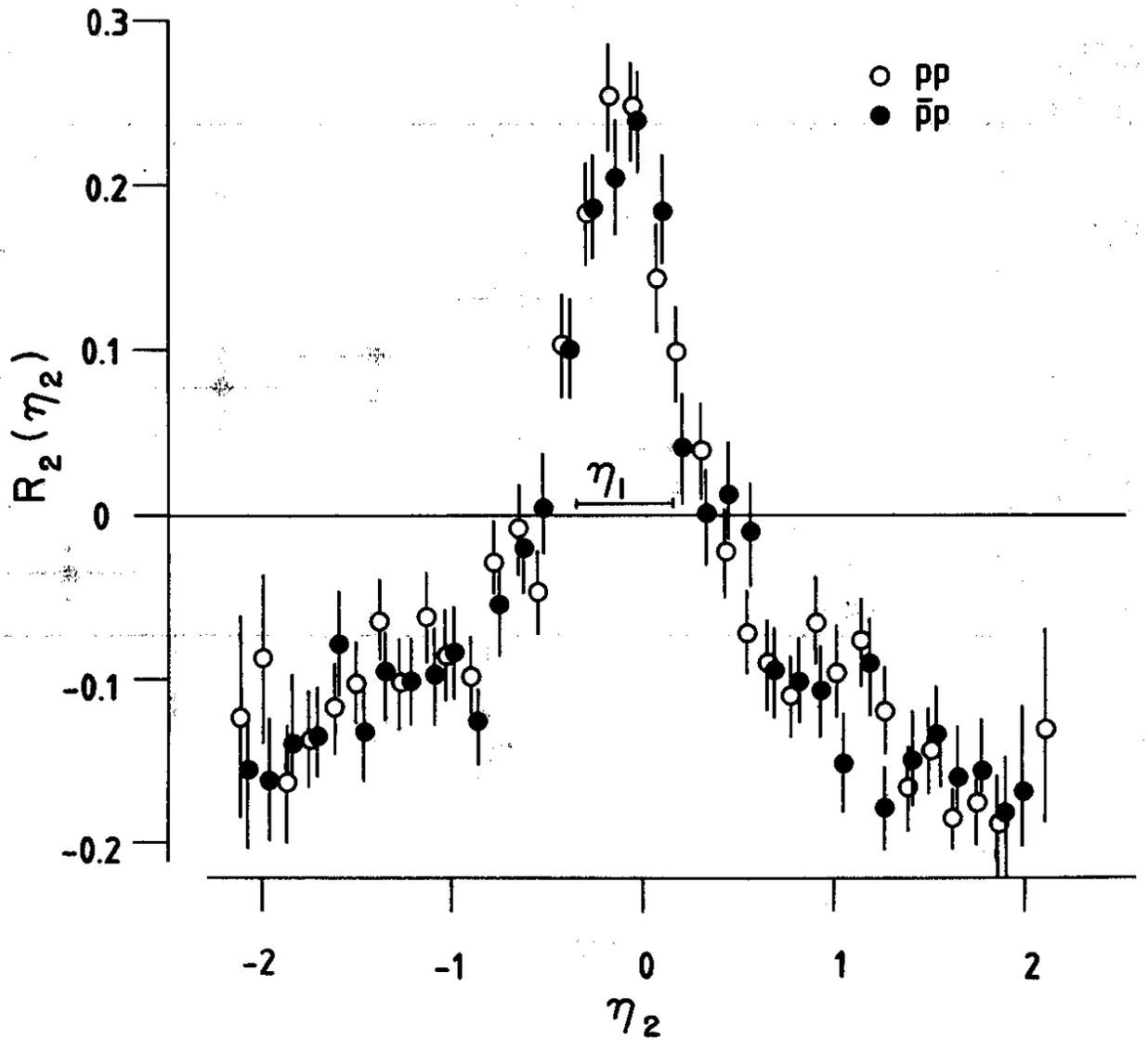

Fig. 4a

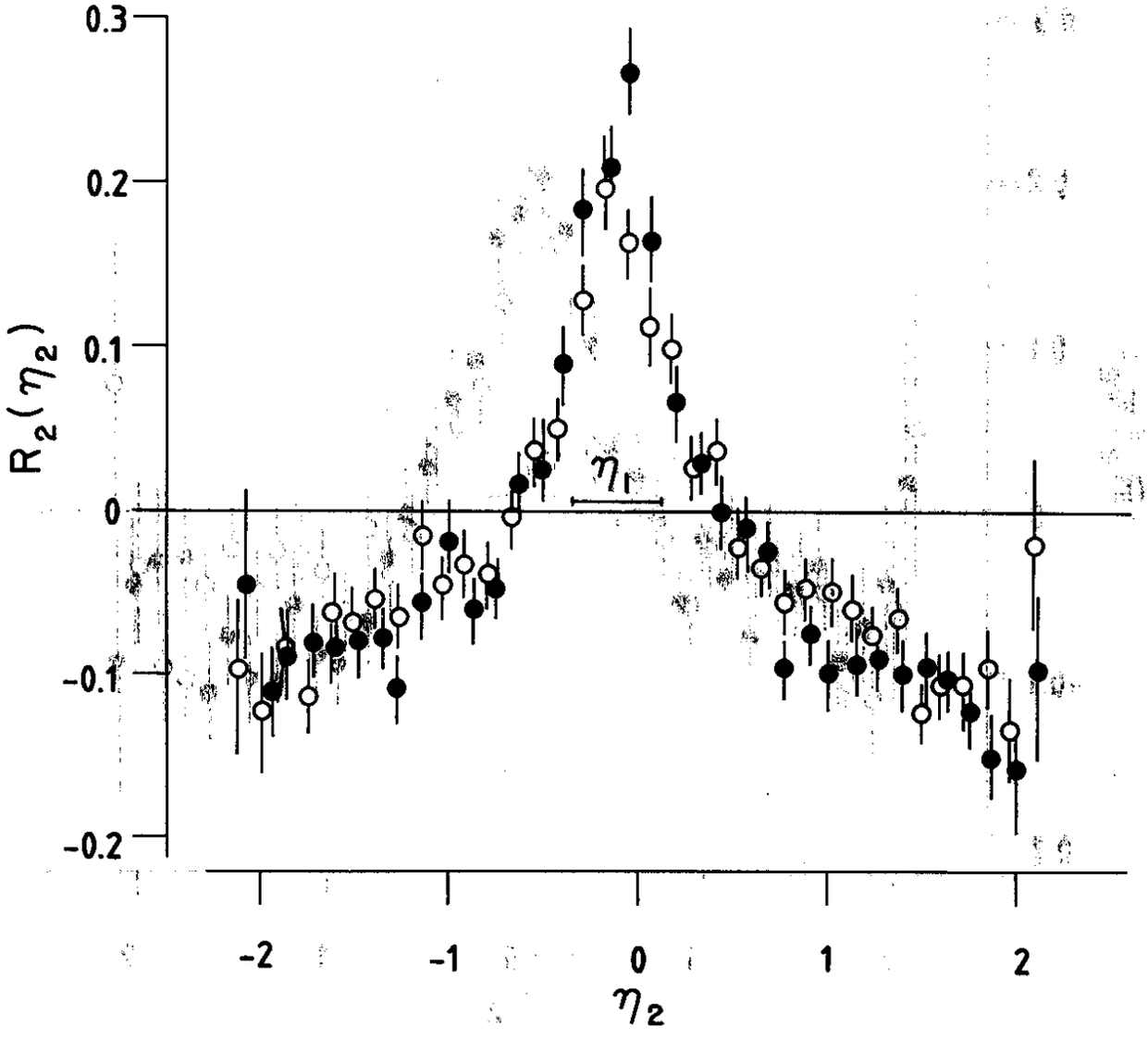

Fig. 4b

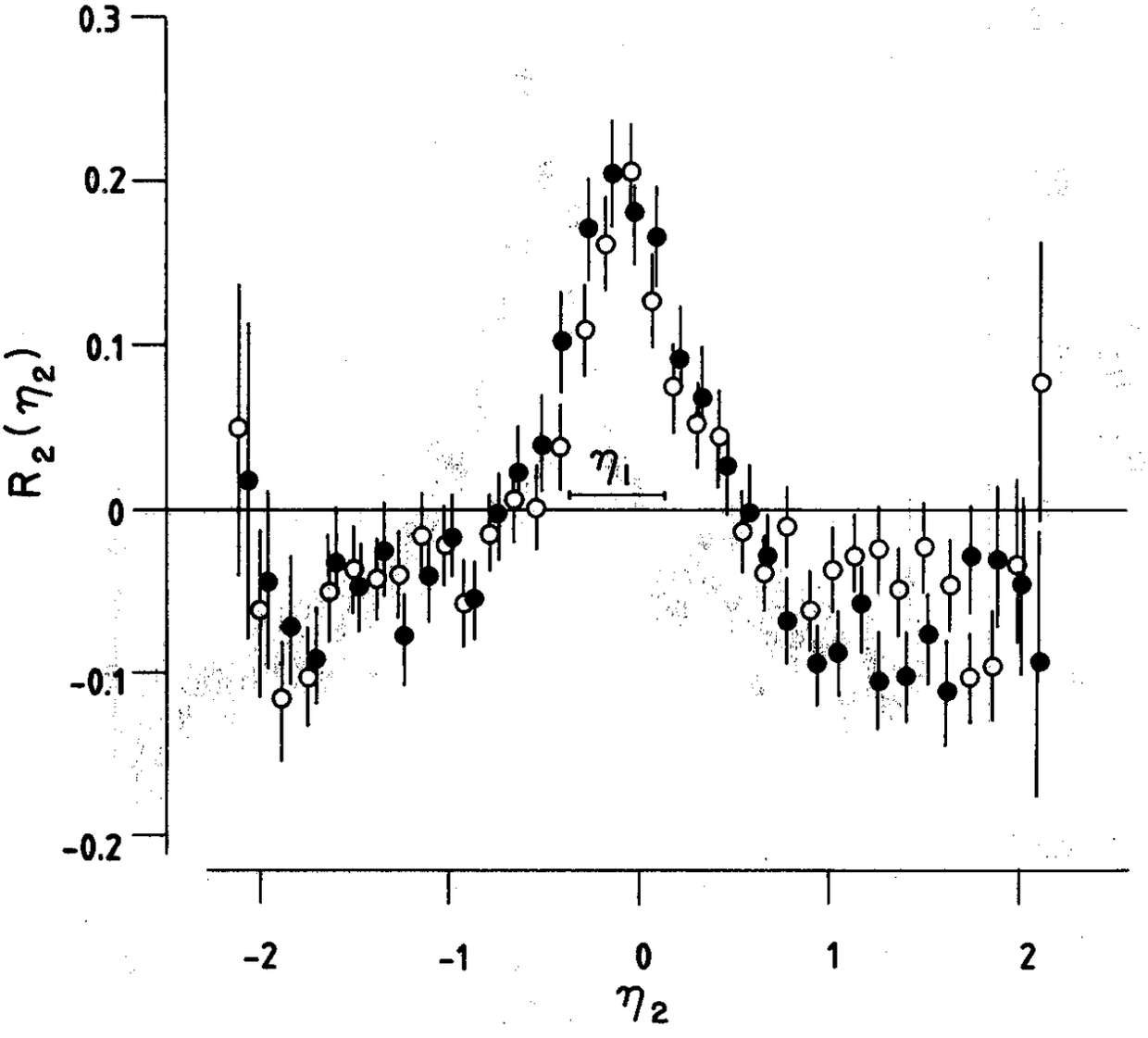

Fig. 4c

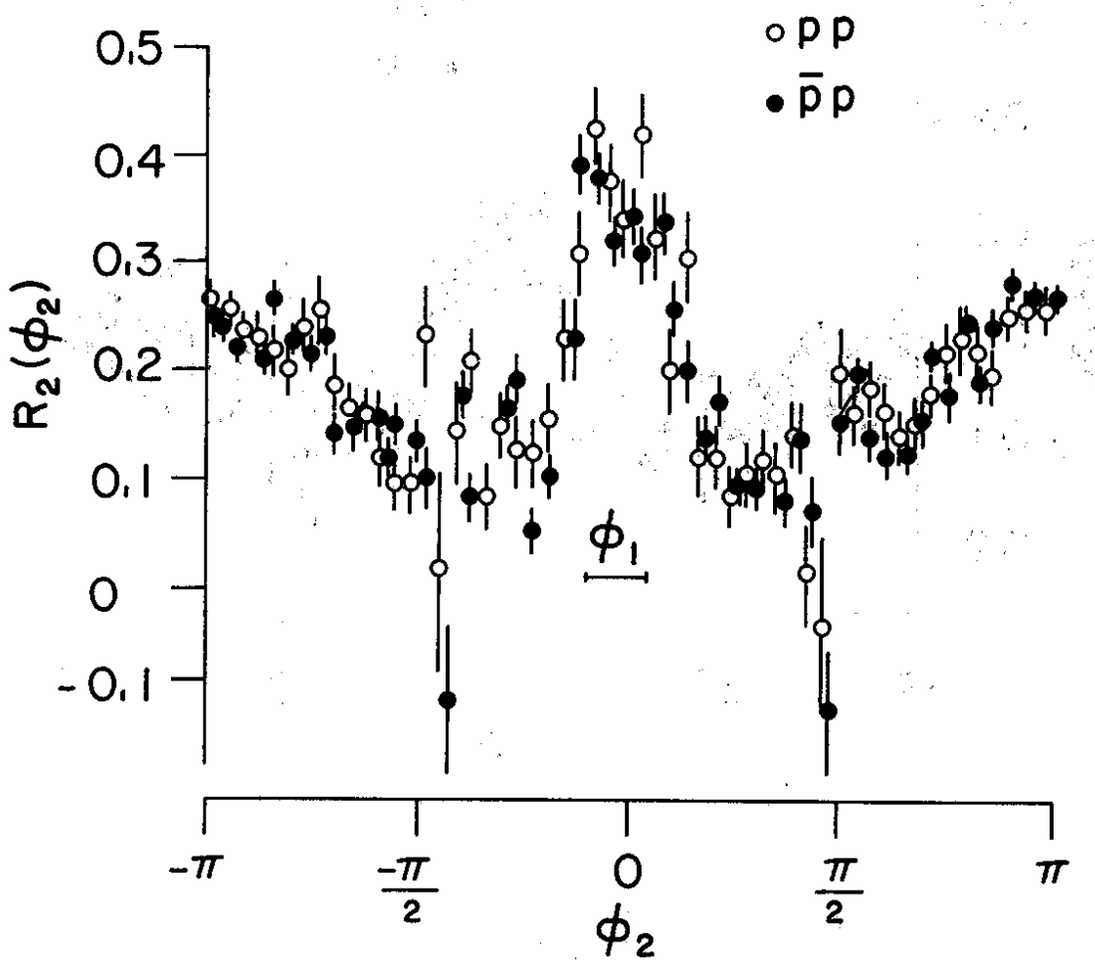

Fig. 5a

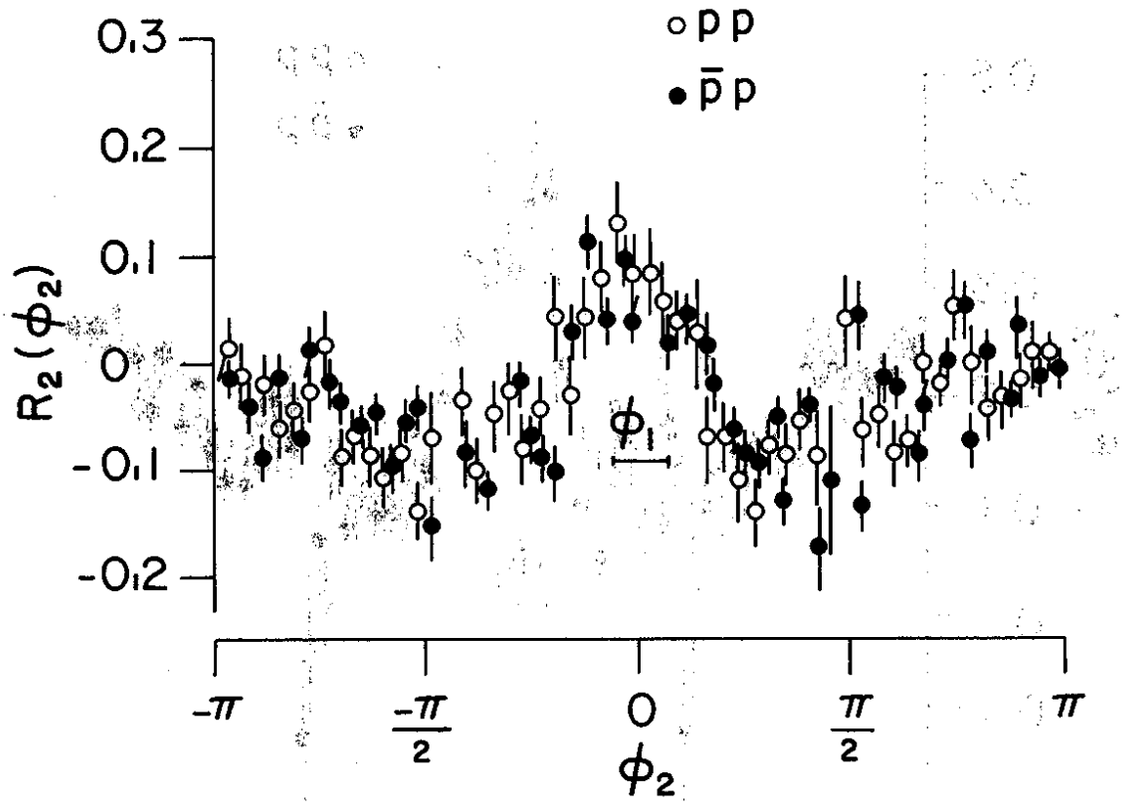
0.3
0.2
0.1
0
-0.1
-0.2
$R_2(\phi_2)$
○ p p
● $\bar{p}$ p
ϕ_1
$-\pi$
$\frac{-\pi}{2}$
0
$\frac{\pi}{2}$
π
ϕ_2

Fig. 5b

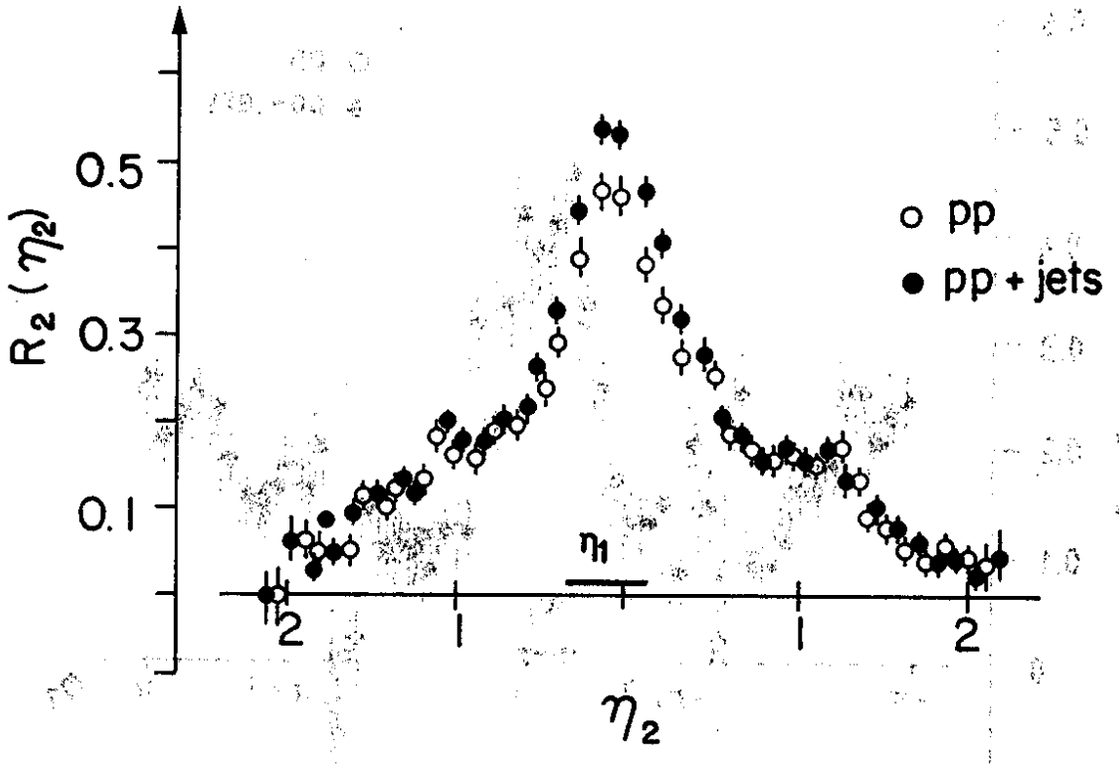

Fig. 6

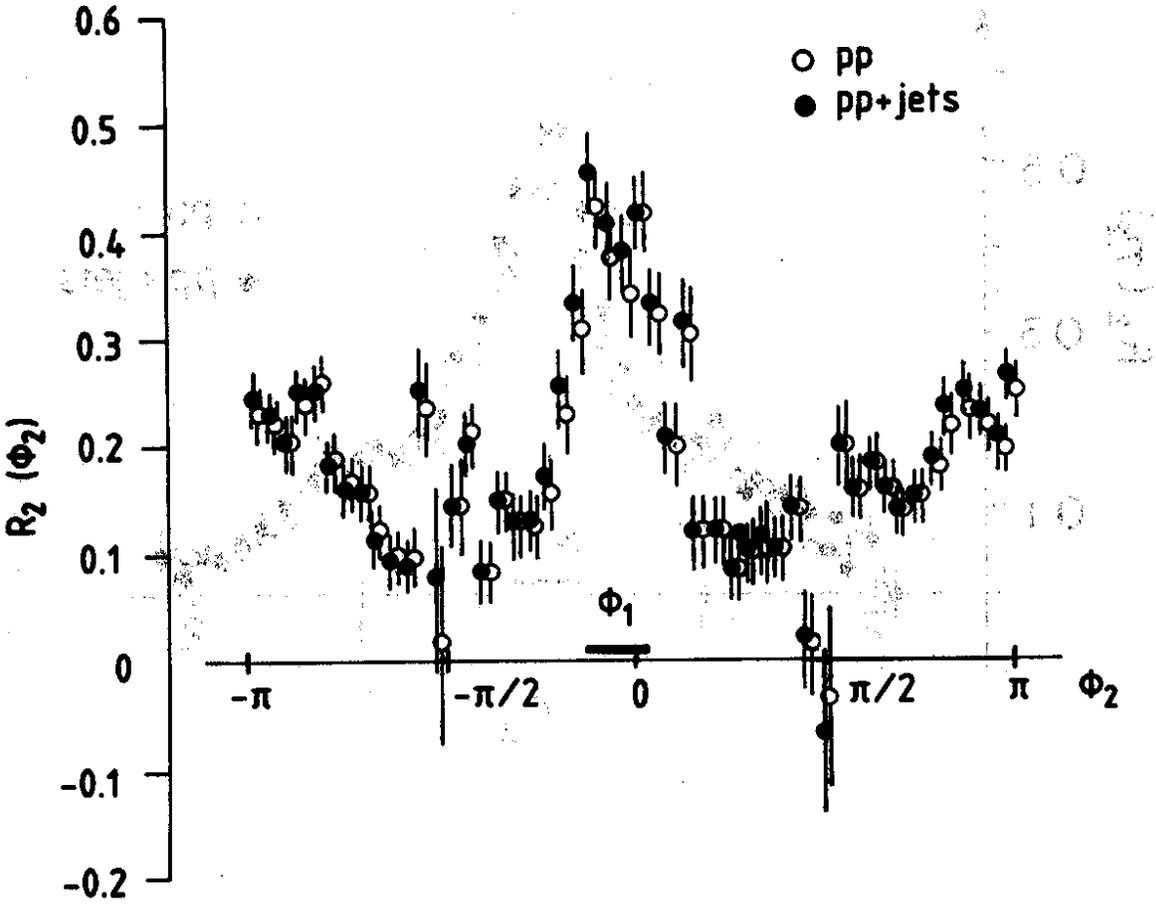
0.6
0.5
0.4
0.3
0.2
0.1
0
-0.1
-0.2
$R_2(\Phi_2)$
pp
pp+jets
Φ_1
$-\pi$
$-\pi/2$
0
$\pi/2$
π
Φ_2

Fig. 7